ACS OMEGA

Open Access



http://pubs.acs.org/journal/acsodf

Article

# Suppression of Hydrogen Sulfide Generation via the Coexistence of Anaerobic Sludge and Goethite-Rich Limonite/Polyethersulfone Composite Fibers

Anh Phuong Le Thi, Reiko Wakasugi, and Takaomi Kobayashi*

Cite This: *ACS Omega* 2023, 8, 35054−35065

Read Online

ACCESS | Metrics & More | Article Recommendations

**ABSTRACT:** Limonite−polyethersulfone (PES) composite fibers were prepared by the wet spinning method to suppress hydrogen sulfide ($H_2S$) generation from anaerobic microbial sludge. The $H_2S$ adsorption of the prepared limonite composite fibers followed the Langmuir type, with a maximum adsorption capacity of 3.7−4.4 g $H_2S$/g, indicating mesopore adsorption. The in vitro $H_2S$ fermentation environment with anaerobic microbial sludge with the coexistence of limonite composite fibers exhibited suppression of $H_2S$ generation. The coexistence of limonite composite fibers also suppressed the amount of CO generation produced by microbial fermentation, so the fibers also affected the metabolism of anaerobic microorganisms. During the anaerobic digestion process, particularly at 672−840 h (28−35 days), the mesopores of limonite in the composite fibers disappeared and changed to macropore adsorption, and the reaction of limonite with hydrogen sulfide produced pyrite ($FeS_2$) and iron sulfate ($Fe_2(SO_4)_3$) as products, which remained in the fiber with conversion efficiencies of 6.8 and 32.4%, respectively. The in vitro hydrogen disulfide action of limonite composite fibers was found to be able to suppress the generated environment of about 300 ppm to about 0.4 ppm.

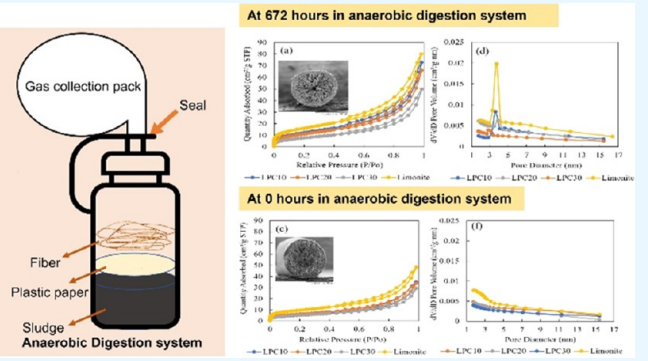


## 1. INTRODUCTION

Hydrogen sulfide ($H_2S$) is an irritant, an asphyxiant gas, and the most toxic, odorous, and highly corrosive among sulfur compounds. Due to being highly toxic,[1] a $H_2S$ level exceeding 400 ppm is life-threatening and that exceeding 500−700 ppm causes staggering and collapse within 5 min with severe eye damage. Single exposure to such high levels can result in death. Even at extremely low concentrations, humans are highly sensitive to the distinct smell of $H_2S$, often described as the odor of rotten eggs.[1] Also, the effect paralyzes the sense of smell at levels above 100 ppm. Inhalation is the primary route of exposure to $H_2S$, as the gas is rapidly absorbed through the lungs. It is crucial to recognize the hazardous nature of this toxic gas and its detrimental impact on human health.[2] Sulfate-reducing bacteria play a role in the natural production of $H_2S$ by reducing sulfur sources found in bottom sediments.[3] These bacteria contribute to the release of $H_2S$ during anaerobic digestion, a process involved in desulfurizing sulfur-containing compounds. This release of $H_2S$ can have an impact on the surrounding environment and its living organisms. For example, in closed sea areas such as the Ariake Sea and Tokyo Bay in Japan,[4] malodorous gas has been emitted at low oxygen concentrations due to the sulfate-reducing bacterium Desulfosarcinaceae, causing problems in people's lives. Also, in unstable low-lying water in Lake Nakaumi, anoxic conditions are likely to produce $H_2S$ by microbial action.[5] In addition, the out-of-area release of $H_2S$ due to industrial accidents is also a source of occupational $H_2S$ exposure to humans.[6−8] In order to avoid the natural odors and hazards that arise from polluted urban water and industrial process sediments in the summer, it is necessary to establish efficient technological controls. These controls are aimed at regulating and minimizing the levels of $H_2S$. Consequently, it is necessary to prioritize the development of effective methods for managing and reducing $H_2S$ concentrations.

On the other hand, some inorganic materials of silicates, active carbon, and zeolite oxide have been recognized for their $H_2S$ adsorption properties.[9,10] For example, adsorbents based on ZnO have been reported to be effective in removing $H_2S$ from biogas.[11] Additionally, several iron-based adsorbents, including Fe, $Fe_2O_3$, and FeOOH, have demonstrated the

Received: June 26, 2023
Accepted: August 30, 2023
Published: September 13, 2023

ability to suppress $H_2S$ emissions with the final product of FeS in the biogas environment.[12−14] The fabrication of such iron hydroxides like FeOOH is typically accomplished through the precipitation method[15] and composited with activated carbon,[16] among the oxides with high reactivity with $H_2S$.

In contrast to such synthetic $H_2S$ removal materials, there exist naturally occurring minerals that have the ability to absorb $H_2S$, making them valuable from a low-carbon perspective. For instance, red rock containing a massive amount of iron in the form of magnetite ($Fe_3O_4$), gothite [FeO(OH)], and hematite ($Fe_2O_3$) is a potential $H_2S$ adsorbent as a natural material.[17] A similar mine in Japan is located in the Aso region of Kumamoto, where limonite is produced. This natural resource, primarily composed of iron oxide, is mainly used for desulfurizing waste gases from biological sewage treatment towers.[18−21] It is known that as a porous material, limonite has excellent adsorption properties toward $H_2S$[21] and exhibits a higher desulfurization activity than other iron ores due to several factors: the higher Fe content, larger surface area and pore volume, and crystal forms. These crystal forms are composed of a large amount of hydrated iron (III) oxide powder, having microcrystalline goethite ($\alpha$-FeOOH) and a small amount of hematite.[18] On the other hand, $\alpha$-FeOOH powder was synthesized using a $FeCl_3$ solution and $NH_4HCO_3$. The results demonstrate that $\alpha$-FeOOH within the composite exhibits a remarkable capacity for $H_2S$ removal from gas streams and the conversion of $H_2S$ into FeS and S.[22] Furthermore, the recovery of powdered limonite from contaminated soil is nearly impossible, and the utilization of large quantities of it is undesirable for several reasons. First, using excessive amounts of the adsorbent can be counterproductive in terms of environmental pollution. Second, the residual adsorbent can lead to secondary environmental contamination.

As seen in the recovery of the fibered zeolite decontaminant during the removal of radioactive cesium,[23] methods for recovering materials have garnered attention. On the other hand, the characteristics of limonite powder, such as large surface area and high desulfurization efficiency, make it advantageous to harness these properties as a desulfurization agent. Therefore, composite desulfurizers that can be recovered while retaining the properties of limonite are valuable as a future innovation technology. For other types of desulfurization, a nanoporous composite sorbent composited with polyethyleneimine and mesoporous molecular sieve has demonstrated remarkable desulfurization characteristics.[24] However, it has been observed that the sorbed $H_2S$ was reduced in the presence of moisture. Under these circumstances, we have proposed limonite polymer composite fibers as a new polymer desulfurization material. In this approach, the wet spinning method, which we have been using, can be utilized to create a porous structure by fibering the material. By doing so, the properties of limonite can be incorporated as a desulfurization agent with minimal reduction. Moreover, the combination of porous polymer fibers and inorganic powder results in a material with a high surface area and effective entangling packing properties for treatment purposes.[25,26] These porous composite fibers fabricated by the wet spinning method[25] using polyethersulfone (PES) exhibited decontamination of radioactive cesium from the environment[27] and heavy metal ions[25] and bleaching of organic dyes.[28] Therefore, as an original attempt, it is interesting to use limonite-composited PES fibers as a desulfurization material for $H_2S$ suppression. The objective of this current research is to produce new polymer limonite composite fibers through the wet spinning technique and assess their performance in removing $H_2S$, as well as their application desulfurization involving $H_2S$-producing soil bacteria. The fibers were collected after treatment from the soil sludge, and a comparison was made between their properties before and after desulfurization through in vitro anaerobic digestion. The sludge environment characteristics also explain the decontaminating of $H_2S$ through anaerobic digestion.

## 2. EXPERIMENTAL SECTION

**2.1. Limonite and Limonite−Polyethersulfone Composite Fibers.** Figure 1 shows limonite powder used as a natural material with a yellowish brown color produced by Nippon Limonite Co., Ltd. at the volcanic eruption of Aso Mountain in Kumamoto Prefecture. *N*-Methyl-2-pyrrolidone (NMP) and other chemicals were purchased from Nacalai Tesque Inc. (Japan) and were used without purification. The

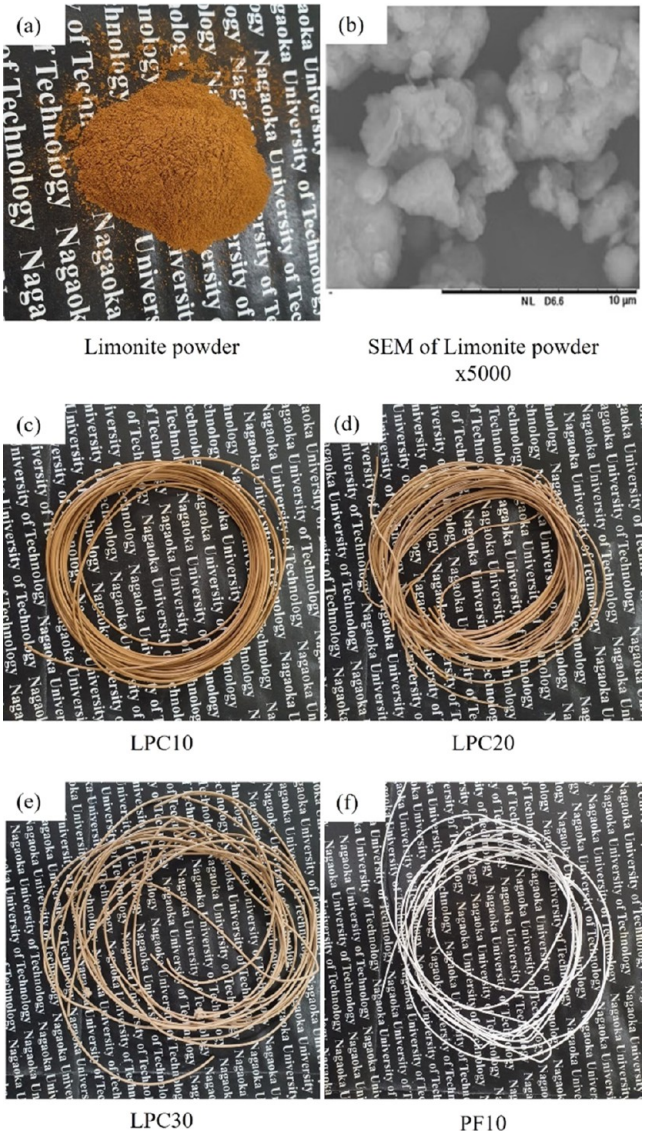


**Figure 1.** Composite fibers after the wet spinning process: (a) limonite powder, (b) SEM of the limonite at 5000× magnification, (c) LPC10, (d) LPC20, (e) LPC30, and (f) PF10.


https://doi.org/10.1021/acsomega.3c04540
ACS Omega 2023, 8, 35054−35065

Table 1. Physical Properties of Limonite, PF10, and LPC Fibers

| sample | NMP [wt %] | PES [wt %] | limonite powder contents [wt %] | diameter [mm] | tensile strength [MPa] | density [g/cm$^3$] | porosity (%) |
|---|---|---|---|---|---|---|---|
| LPC10 | 90 | 10 | 60 | 0.68 | 6.0 ± 0.8 | 0.815 | 21.76 |
| LPC20 | 80 | 20 | 60 | 0.75 | 8.9 ± 0.4 | 0.944 | 12.93 |
| LPC30 | 70 | 30 | 60 | 0.78 | 2.9 ± 0.9 | 1.269 | 7.48 |
| PF10 | 90 | 10 | 0 | 0.65 | | 0.778 | 4.4 |
| limonite | | | 100 | 0.03 | | | |

dried limonite powders were crushed and passed through a 30 $\mu$m sieve. Polyethersulfone (PES, Ultrason E2010) was a BASF Co., Ltd. (Germany) product.

In our previous procedures,[25,26] the wet spinning process for fabricating fibers was performed for PES−NMP solutions with suspended limonite powders. When PES solution containing limonite powder was mixed with PES, the viscous solution was applied for wet spinning by squeezing out into the water medium placed at the bottom under pressure and forming fibers in the water medium at room temperature.[25,27,29] Here, PES was dissolved in NMP at 10, 20, and 30 wt % concentrations, and then, 60 wt % limonite powder against the weight amounts of the PES was added to the NMP solution. Then, the mixed solution was extruded through a cylindrical needle with a 0.8 cm diameter and placed in a 200 mL volume metal cylinder with a cylindrical needle of 0.8 cm diameter at the bottom in the 10 L water tank prepared below the needle. The mixed solution was extruded at a pressure of 0.42 MPa, and the insoluble PES−limonite solidified in the water because NMP in the mixed solution dissolved at 298 K. Then, the fibrous limonite PES composite (LPC) formed in the lower water tank was further transferred to another tank and rinsed with large amounts of water at 353 K to remove residual NMP. Finally, the fibers were dried under vacuum at 333 K. Fibers formed at PES concentrations of 10, 20, and 30 wt % with a fixed limonite amount of 60 wt % were named LPC10, LPC20, and LPC30, respectively (Figure 1). As a comparison, 10 wt % PES fibers without limonite as PF10 were prepared similarly.

**2.2. Characterization of Limonite Powder and LPC Fibers.** To investigate the changes in the morphology of the fiber, a scanning electron microscope (SEM, TM3030Plus HHTC, Japan) at an accelerating voltage of 15 kV was used for gold-sputtered samples. The surface area of limonite and the composite fibers was measured by the Brunauer−Emmer−Teller (BET) method using a Tristar II 3020 (Micromeritics Inc. TriStar II, Shimadzu, Japan). Before measurement, samples were degassed by vacuum overnight at 70 °C. The density of the composite fibers was determined by the Archimedes method. A dry specimen with known weight was immersed in excess water until the specimen in the water reached equilibrium. The density of prepared specimens ($\rho$) was calculated by $\rho = \frac{W_s}{W_s - W_w} \times (\rho_o - d) + d$, where $\rho$ is the density (g/cm$^3$), $W_s$ denotes the specimen weight in air (g), $W_w$ represents the specimen mass in ethanol (g), $\rho_o$ is the density of ethanol (g/cm$^3$), and d is the density of air (g/cm$^3$). In transmittance mode, the Fourier transform infrared (FT-IR) spectra of limonite powder and the composite fibers were measured with an IRPrestige-21 (Shimadzu Co., Ltd). The transmission spectra were obtained by forming a thin KBr-PPy pellet. The FT-IR spectra were obtained with 16 scans from 400 to 4000 cm$^{-1}$ using the resolution of the spectral measurements at 4.0 cm$^{-1}$. The tensile strength of the LPC fibers was measured using a load measurement device (LTTU-500N, Minebea Co. Ltd., Japan) with an operating head loading of 500 N at 23 °C with 50 %RH. The gauge length and the crosshead speed were 30 mm and 2 mm/min, respectively. Five specimens were tested for each sample. Each instance had a 50 mm length. First, the diameter of each piece was measured using a micrometer (Mitutoyo 103−177, Japan) to calculate the cross-sectional surface area. According to the following equations, tensile strength and elongation were calculated: tensile strength (MPa) = maximum load/cross-sectional area and elongation (%) = 100 × (elongation at rupture/initial gauge length). X-ray diffraction (XRD) spectra of limonite and composite fibers were analyzed with a SmartLab X-ray diffractometer (Rigaku Corporation) using Cu K$\alpha$ radiation ($\lambda$ = 1.5406 Å). XRD patterns were recorded over a 2$\theta$ range from 10 to 70° with 40 kV and 30 mÅ. An X-ray fluorescence analyzer (ZSX Primus II (Rigaku Corporation, Japan)) was used for limonite and composite fiber component analysis. A 10 mm diameter pellet was made using limonite, composite fibers, and an aluminum ring using a hydraulic compress with 450 kgf/cm$^{-2}$ pressure for the measurement.

**2.3. Measurements of the Adsorption Isotherms of $H_2S$ and Preparation of Waste Sewage Sludge Having Anaerobic Microorganisms.** $H_2S$ adsorption experiments were performed in the following two patterns. In the first, samples were placed in $H_2S$ gas at different concentrations, and the adsorption amount of $H_2S$ was examined. In another way, the composite fiber was placed with the sludge of an anaerobic microbial medium producing $H_2S$, and the amount of $H_2S$ produced was measured. In former experiments, limonite powders or composite fibers were initially subjected to vacuum overnight at a temperature of 343 K. Subsequently, a gas adsorption test was performed inside a 1 L glass three-necked flask, which was sealed and vacuumed with a vacuum pump. Then, the vacuum was sealed, and the $H_2S$ gas was generated with the chemical reaction $CaS + 2H_3PO_4 \rightarrow H_2S + Ca(H_2PO_4)_2$ by utilizing a $H_2S$ generation tube (GASTEC No. HSC-21L, 21, and 21H) kept in a 20 L plastic bag. Then, the $H_2S$ gas was transferred to the sealed flask at concentrations of 4, 16, 85, and 310 ppm. Finally, measurements of $H_2S$ concentrations were performed using a multi-gas detector when the PES−limonite samples (g) were placed in the flask.

On the other hand, for the latter case of anaerobic digestion in vitro, experiments using anaerobic microbes could generate $H_2S$ when the medium was incubated in anaerobic plastic bottles with subsequent addition of nutrients. Here, waste sewage sludge collected from the Akemi estuary mouth in Nishi-ku, Kumamoto city in Japan, was cultured anaerobically in plastic bottles. First of all, into the sewage, sludge samples containing sulfate-reducing bacteria, gypsum ($CaSO_4$), and starch ($(C_6H_{12}O_5)_n$) were added in a 250 mL plastic bottle with a lid seal. All vials were hermetically sealed with a butyl rubber stopper on the top lid, facilitating anaerobic conditions.


https://doi.org/10.1021/acsomega.3c04540
ACS Omega 2023, 8, 35054−35065

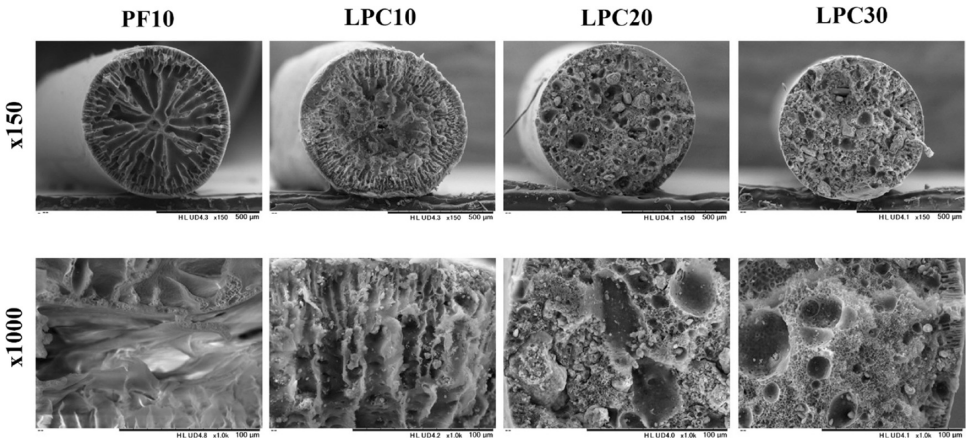


**Figure 2.** SEM images of the cross section of PF10 and the composite fibers at 150× and 1000× magnifications.

Then, a predetermined amount of PES−limonite fibers was added to each bottle, the microorganisms were incubated at 20 °C, and the amount of $H_2S$ produced was measured. The experiments were conducted at a temperature of 20 °C. During the incubation, $H_2S$ and carbon monoxide (CO) gas concentrations were measured using a multi-gas detector. The sample gas was measured by aspirating the gas inside the bottle through a suction port with a rubber stopper on the top lid.

## 3. RESULTS AND DISCUSSION

**3.1. Characterization of Limonite Composite Fibers as $H_2S$ Adsorbents.** As shown in Figure 1, the composite fibers fabricated using the coagulation process of PES dissolved in NMP solution could produce thin fibers with the ochre color of limonite, compared to the white color of PES fibers. Table 1 provides an overview of the characteristics of each sample. The density of the composite fibers (LPC10, LPC20, and LPC30), which had a fixed limonite content of 60 wt % and varying PES concentrations (10, 20, and 30 wt % relative to limonite, respectively), increased with higher PES concentration. The BET surface area values determined through nitrogen adsorption exhibited a tendency to increase in LPC30, LPC20, and LPC10. These results indicate that the increase in PES concentration during fiber formation influences the porosity of the resulting fibers.

Figure 2 depicts an SEM image of the cross section of resultant composite fibers. The cross-sectional photographs of the fibers reveal that the diameter of each fiber is approximately 650−780 $\mu$m. The images clearly showed the structural variations in porosity within the fiber at different PES concentrations. In other words, in the PES-only fiber, a pleated structure with a width of about 10 $\mu$m was observed from the center of the fiber toward the surface. This suggests that the coagulation of PES caused structural changes as water gradually penetrated the fiber from the surface to the interior during fabrication. On the other hand, the fabricated PF10 had a morphology structure with large pores radially extending and spreading outward from the center of the fiber toward the periphery. This indicated that PES coagulated from the surface to the center by water penetration, resulting in solvent exchange with the water. In contrast, in LPC10, which contained 60 wt % limonite in a 10% wt PES−NMP solution, small radially elongated pores were observed near the surface in the SEM photograph. However, the center of the cross section looked like a denser agglomerate, indicating that the porosity of LPC10 was less than that of PES. This could be attributed to the presence of limonite powder hindering PES coagulation, causing slower solidification of PES in water. For LPC20 and LPC30, the structure became denser, with both limonite powder and PES forming tiny round pores in a sponge-like structure. The limonite particles with a diameter of less than 30 $\mu$m were uniformly distributed within the fiber structure, and the micrograph observation of the fiber cross section showed that PES was saved as an embedded limonite powder in the fiber. Based on the data presented in Table 2,

**Table 2. Surface Area, Pore Volume, Pore Size, and Elemental Composition of Limonite and LPC Fibers at 0 h**

| | | | | elemental composition | | |
|---|---|---|---|---|---|---|
| sample | BET surface area ($m^2/g$) | BJH adsorption average pore volume ($cm^3/g$) | BJH adsorption average pore size (nm) | C/Fe | Si/Fe | S/Fe |
| limonite | 59.37 | 0.078 | 4.29 | 0.15 | 0.13 | 0.03 |
| LPC10 | 41.82 | 0.043 | 4.84 | 1.89 | 0.09 | 0.36 |
| LPC20 | 36.88 | 0.040 | 4.83 | 2.33 | 0.2 | 0.36 |
| LPC30 | 32.26 | 0.034 | 5.8 | 2.57 | 0.017 | 0.57 |
| PF10 | 6.05 | 0.012 | 5.35 | | | |

the ratios of carbon, iron, and sulfur components in the fabricated fibers were determined using XRF analysis. The C/Fe values were found to be 1.89, 2.33, and 2.57 for LPC10, LPC20, and LPC30, respectively. These findings clearly indicated that the denser structure of LPC30 contained higher amounts of PES than LPC10, as evidenced by the higher carbon content in LPC30. It is worth noting that the result suggested that higher concentrations of PES relative to limonite like LPC30 formed a denser internal fiber structure. As shown in Table 2, the BET surface area of all materials at 0 h tends to decrease from 41.8 $m^2/g$ for LPC10 to 32.3 $m^2/g$ for LPC30. However, the surface area values of PF10 and limonite powder were 4.4 and 59.4 $m^2/g$, respectively. Hence, the surface area of the composite fiber decreases with increasing PES concentration. Additionally, the inclusion of limonite powder, which has the largest surface area, was reduced in the composite fiber. Figure 3 shows the adsorption isotherms of $H_2S$ gas with different concentrations of 0, 5, 15, 85, and 310 ppm for composite fibers and limonite powder.



https://doi.org/10.1021/acsomega.3c04540
ACS Omega 2023, 8, 35054−35065

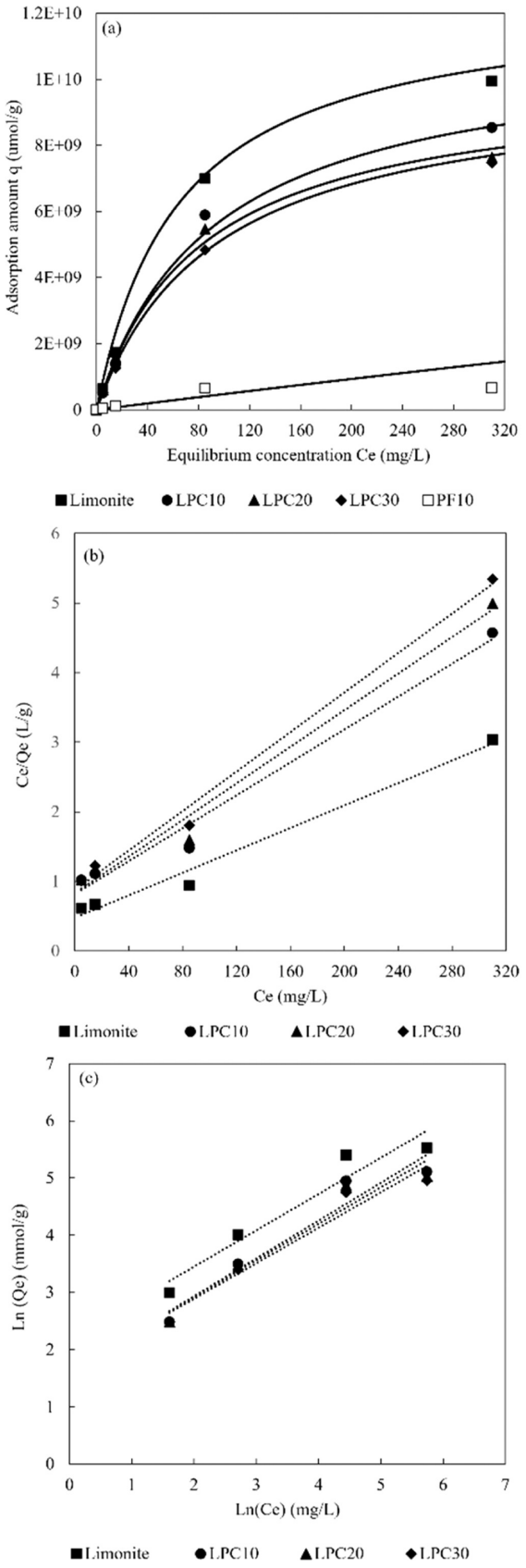


**Figure 3.** $H_2S$ isothermal plots of the adsorption amount (q) versus equilibrium concentration of $H_2S$ (a), Langmuir model (b), and Freundlich model (c) for $H_2S$ gas adsorption of limonite and composite fibers plots.

The adsorption isotherms of $H_2S$ gas in limonite and composite fibers displayed an initial rapid increase in the low concentration range, followed by a linear isotherm at higher concentrations. Limonite exhibited the highest adsorption capacity for the $H_2S$ gas, while PF10 fibers without limonite showed a low adsorption capacity. When comparing LPC10, LPC20, and LPC30, LPC10 absorbed the next highest amount of limonite, followed by LPC20 and LPC30 in decreasing order. The results in Table 1 demonstrated that LPC10 fibers had a higher surface area than LPC20 and LPC30, suggesting that a more porous structure could be kept in LPC10 by enveloping it with the PES porous scaffold, causing high adsorption of $H_2S$. To investigate the adsorption mechanism, the experimental data for $H_2S$ adsorption were analyzed by plotting with Langmuir and Freundlich, as shown in Figure 3 (b) and (c), respectively. The calculated parameters and correlation coefficients $R^2$ are listed in Table 3.

**Table 3. Parameters of Langmuir and Freundlich Isotherms and Comparison with Other Works**

| | isotherm models | parameter | |
|---|---|---|---|
| limonite | Langmuir | $Q_m$ (g $H_2S$/g) | 4.42 |
| | | $K_L$ | 3.69 |
| | | $R^2$ | 0.98 |
| | Freundlich | $K_f$ (g $H_2S$/g) | 24.82 |
| | | $N$ | 0.68 |
| | | $R^2$ | 0.93 |
| LPC10 | Langmuir | $Q_m$ (g $H_2S$/g) | 3.74 |
| | | $K_L$ | 5.52 |
| | | $R^2$ | 0.98 |
| | Freundlich | $K_f$ (g $H_2S$/g) | 25.84 |
| | | $N$ | 0.7 |
| | | $R^2$ | 0.94 |
| LPC20 | Langmuir | $Q_m$ (g $H_2S$/g) | 3.4 |
| | | $K_L$ | 6.05 |
| | | $R^2$ | 0.98 |
| | Freundlich | $K_f$ (g $H_2S$/g) | 25.84 |
| | | $N$ | 0.68 |
| | | $R^2$ | 0.94 |
| LPC30 | Langmuir | $Q_m$ (g $H_2S$/g) | 3.4 |
| | | $K_L$ | 6.48 |
| | | $R^2$ | 0.99 |
| | Freundlich | $K_f$ (g $H_2S$/g) | 25.84 |
| | | $N$ | 0.66 |
| | | $R^2$ | 0.94 |
| 20Fe−CNF[30] | | $Q_m$ (g $H_2S$/g) | 0.72 |
| ZnO−CuO dispersed AC[11] | | $Q_m$ (g $H_2S$/g) | 0.05 |
| coconut shell-based AC[31] | | $Q_m$ (g $H_2S$/g) | 0.125 |
| N-doped mesoporous carbons[32] | | $Q_m$ (g $H_2S$/g) | 2.94 |
| alkaline graphene aerogel[33] | | $Q_m$ (g $H_2S$/g) | 3.39 |

The correlation coefficient obtained in the Langmuir plot was higher than that of the Freundlich plot, suggesting that the Langmuir isotherm model provided a better fit for the experimentally obtained results for $H_2S$ adsorption. Since $H_2S$ adsorption did not occur with PF10, this result could be interpreted as $H_2S$ adsorption being expressed in the limonite portion of the fiber. The maximum adsorption capacities ($Q_m$) of limonite, LPC10, LPC20, and LPC30 were 4.42, 3.74, 3.4, and 3.4 g $H_2S$/g, respectively. The adsorption capacity value was compared with other adsorbents taken from the literature


https://doi.org/10.1021/acsomega.3c04540
ACS Omega 2023, 8, 35054−35065

in Table 3. This comparison showed that limonite and composite fibers exhibited higher adsorption capacities to $H_2S$ than $Fe_2O_3$-supported SBA-15, Fe nanoparticles, ZnO−CuO N-doped mesoporous carbons, and coconut shell-based AC having $Q_m$ values of 0.05, 0.125, 294, and 3.39 g $H_2S$/g, respectively.

### 3.2. Suppression Effect of Limonite Composite Fibers on $H_2S$ Releasing from Anaerobic Microbacteria Media.

As a substantive characterization of limonite composite fibers, we conducted an investigation on the temporal variation of $H_2S$ production when the composite fibers were placed into an anaerobic environment. The relationship between the amount of $H_2S$ generated and time in that in vitro experiment is shown in Figure 4. In each experiment, the sludge quantity was maintained at 50 g, and a specific amount of composite fibers (10 g) was added to the incubation medium. As shown in Figure 4, the control sample generated $H_2S$ on increasing the cultivation time, with the concentration reaching 223 ppm after 1176 h for 49 days. A similar trend of $H_2S$ formation was also observed when 10 g of PF10 was added. However, as limonite powder, LPC10, LPC20, or LPC30 was added to each medium, the amount of $H_2S$ generated was almost suppressed. For instance, in the case of limonite and LPC10, no $H_2S$ formation was observed until 504 h, after which it gradually increased until reaching 33 ppm at 1176 h.

In contrast, LPC20 and LPC30 exhibited a similar pattern to $H_2S$ generation, reaching approximately 50 ppm at 1176 h. However, till 336 h for 14 days, a lower level of $H_2S$ generation was observed. As anaerobic fermentation of microorganisms also produces CO as a byproduct, simultaneous measurements of CO were conducted along with $H_2S$, as shown in Figure 4(b). CO release was the highest for the control, followed by PF10.

However, both the limonite powder and the composite fibers also demonstrated a reduction in CO emission. The decrease in the CO generation followed a similar trend as that of $H_2S$ generation, meaning that the suppressed production of $H_2S$ might also suppress the metabolism of anaerobic microorganisms. In the control sample, the CO emission at 1176 h was 276 ppm, but in limonite, it was almost 56 ppm, roughly 1/5 of the original CO emission. Similar in vitro experiments were performed with varying amounts of fibers. Figure 5 shows the relationship between the amount of $H_2S$ generated after 672 h and the amount of fibers used. Here, the $H_2S$ generated was observed at 672 h for 28 days of cultivation of 50 g of sludge under anaerobic microorganism conditions, with fiber amounts ranging from 0.5 to 15 g.

Among the effects of different amounts of the limonite composite fibers in the cultivation media, the control without limonite composite fibers generated 114 ppm $H_2S$. However, when LPC10 was added to 0.5 g of the medium, the amount of $H_2S$ production dropped to 79 ppm, reducing the amount by about one-half, and when 15 g of fibers were added to the medium, the amount of $H_2S$ produced was 0.4 ppm; the same trend was also observed for LPC20 and limonite powder.

As a result, the presence of limonite fibers or limonite powder in the anaerobic medium significantly reduces the production of $H_2S$. As noted in Figure 4(b) for CO emissions, monitoring under control conditions exhibited $H_2S$ generation along with the formation of CO, indicating improved anaerobic growth. In contrast, addition of limonite composite fibers or limonite decreased the CO formation, indicating restriction of the ability of anaerobic microbial action.

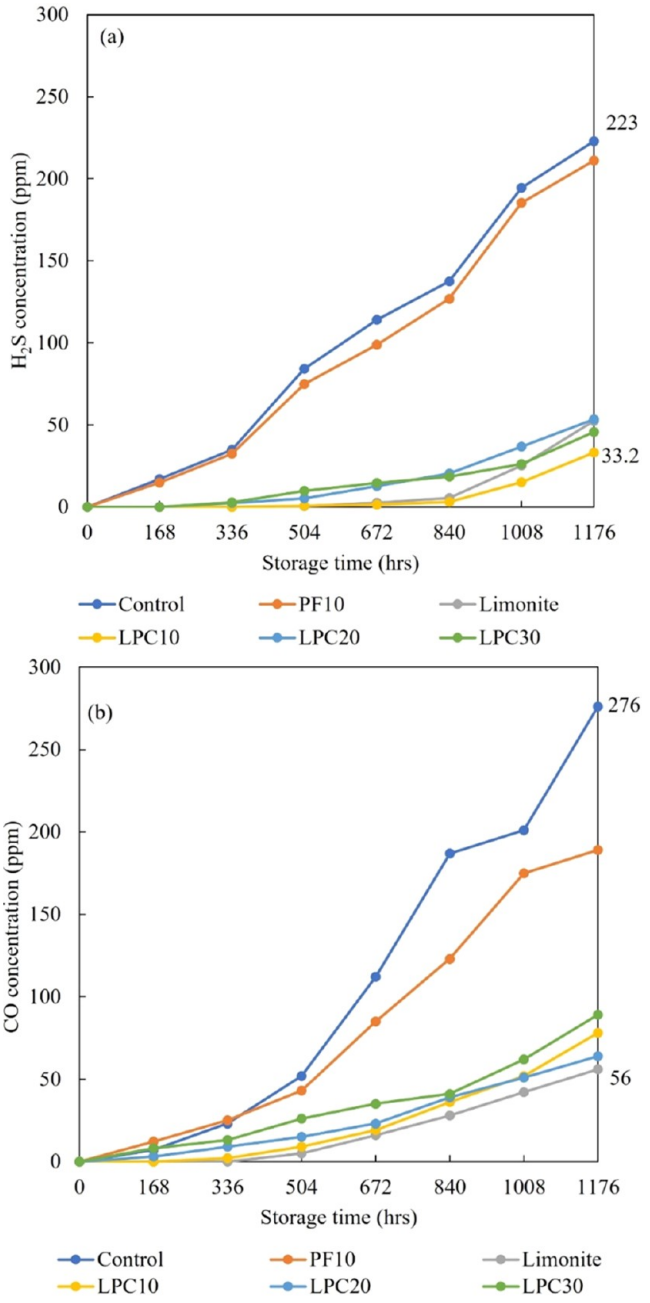


**Figure 4.** Effect of LPC fibers on gas production of $H_2S$ (a) and CO (b) in the presence of composite fibers stored at 20 °C for different times.

On the other hand, to investigate the $H_2S$ suppression by the limonite composite fibers, the properties of fibers used for $H_2S$ removal in the anaerobic medium were characterized as collected from the anaerobic medium after 336 and 672 h. Figure 6 presents SEM and energy-dispersive X-ray spectrometry (EDS) images of the cross section of the fiber used for $H_2S$ removal in anaerobic media with 50 g of sludge. The fiber structure exhibited noticeable changes, particularly in PF10 and LPC10, compared to Figure 2. After 336 h, the PF10 fiber showed collapsed large radial pores, and as the time increased from 336 to 672 h, only the center exhibited visible space. In LPC10, the initial cross-sectional structure seemed to be maintained at 336 h, but some space appeared. Conversely, the cross-sectional structures of LPC20 and LPC30 seemed to


https://doi.org/10.1021/acsomega.3c04540
ACS Omega 2023, 8, 35054−35065

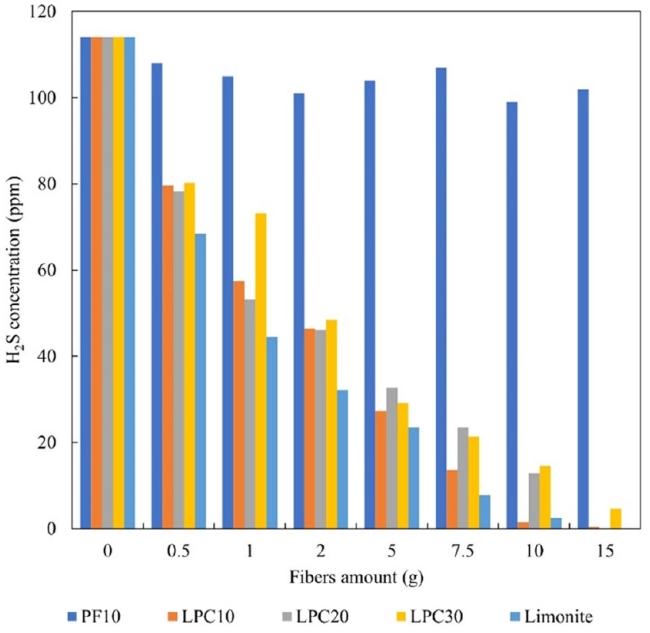


**Figure 5.** Effect of the amount of fibers on the production of $H_2S$ in the presence of the composite fibers stored for 672 h at 20 °C.

remain the same, but the increase in processing time to 672 h increased the density of the cross section. At 1000× magnification, the sponge structure seemed to have disappeared. Figure 7 shows $N_2$ isotherm curves and pore size distribution for the incubated samples.

Table 4 lists X-ray fluorescence (XRF) results for the treated samples incurvated with the sludge for 336 and 672 h. In the composition of the fibers, it was suggested that the Si-to-Fe ratio in each fiber remained at relatively similar values throughout the duration of 336 and 672 h. For instance, in the LPC10 sample, the ratios of Si/Fe were recorded as 0.09, 0.13, and 0.11 for 0, 336, and 672 h, respectively. This indicated that there was no significant penetration of sludge soil into the fibers during the experimental period. In contrast, the C/Fe ratio tended to decrease in the fibers, but limonite increased. In the case of fibers, this could be attributed to a decrease in microbial content, affecting the metabolism of anaerobic microorganisms. On the other hand, S/Fe values also tended to decrease with the increase of the incurvation time in anaerobic media. Furthermore, examination of the EDS images revealed the presence of Si elements in all of the composite fibers. However, in line with the XRF results, the presence and distribution of Si elements remained consistent and uniformly spread across the entire surface area of the composite fibers.

Figure 7 presents the $N_2$ adsorption isotherms of non-incubated (a) and incubated for 336 h (b) and 672 h (c), with the corresponding pore size distributions in (d–f). In Figure 7(a), the $N_2$ adsorption isotherm for limonite exhibits the IUPAC type 4 isotherm, indicating mesopore adsorption. In other fibers, the curve obeyed similar types of isotherms, and the pore diameter distribution had a peak at about 4 nm. However, for both cases of fibers used in the anaerobic treatment for (b) 336 and (c) 672 h, the amount of adsorbed $N_2$ became much lower, and the isotherm followed IUPAC type 2 with macropore adsorption. This finding is consistent with the SEM observations, which also reveal clogging of the nm-sized pores. Furthermore, the BET surface area results in Table 4 demonstrate a substantial reduction in the surface area of all fibers used in the anaerobic treatment. This decline in the surface area further supports the presence of pore clogging in the case of mesopores of the limonite portions. However, the sulfur source cannot be explained solely by XRF results and EDS observation. In other words, if it transforms into Fe–S, as indicated by the original XRF elemental analysis values, no further investigation was conducted through FT-IR analysis.

Figure 8 compares the FT-IR spectra of the limonite powder, LPC fibers, and dry sludge for each aerobic treatment stage. Due to the powdery nature of the limonite powder dissipated during the experiment, it was placed in a mesh bag and put on top of the culture sludge. When comparing the spectra of PF10 used in anaerobic conditions in the presence of $H_2S$ for 336 and 672 h, no significant changes were observed, indicating that PES decomposition did not occur even in a hydrogen sulfide atmosphere.

In contrast, for limonite powder in Figure 8(a), broad peaks observed in the 3400–3200 $cm^{-1}$ range and the peak at 1630 $cm^{-1}$ indicate the stretching vibration of O–H bonds in $\alpha$-FeOOH. The absorption bands at 490 $cm^{-1}$, commonly observed, are associated with the stretching vibrations of Fe–O bonds. By comparing the IR spectra of limonite with those of the composite fibers, a shift was observed in all composite fibers, as seen in (a), attributing to the interaction between PES and limonite. Limonite powder placed in a $H_2S$ atmosphere at 336 and 672 h gave different broad peaks at 1108 $cm^{-1}$. The spectrum of limonite powder stored in a mesh bag showed a significant change in absorption, especially in the 900–1200 $cm^{-1}$ region. Namely, the spectra at 336 and 672 h showed the appearance of an absorption peak of $FeSO_4$ with a sharp absorber at 1102 $cm^{-1}$. Such a change was also observed in LPCs. Also, other bands that appeared at 1159 and 603 $cm^{-1}$ were attributed to Fe═S and Fe–S, respectively.[34] However, the Fe–S band intensity was weaker than that of S═O absorption, which was assigned to $FeSO_4$, suggesting that most of the $H_2S$ sulfur was converted to sulfate ions.

Figure 9 shows the XRD results of composite fibers. For the XRD patterns, sharp diffraction peaks were observed at 28.45, 33.7, and 36.8°, as characterized for goethite $\alpha$-FeOOH[35] at 40.17° to hematite. These patterns were also observed in limonite composite fibers. At 336 and 672 h, these sharp peaks were seen in each XRD pattern, but the appearance of strong, sharp peaks at 33.2, 43.8, and 53.39° corresponding to the (200), (220), and (311) planes, respectively, suggested the presence of $FeS_2$.[36] Furthermore, the sharp peaks appearing at 43.7, 57.2, and 64.9° corresponding to (102), (110), and (201) planes, respectively, provide evidence for the presence of FeS.[37] Moreover, some weak peaks appear at 17.42, 26.79, and 34.89° corresponding to the presence of $FeSO_4$ (mp-19254).[38]

As discussed so far, $H_2S$-generating sludge showed significant $H_2S$ suppression. The adsorption of $H_2S$ into the mesopores of limonite embedded in PES fibers was shown to be affected by the absorbed $H_2S$ forming $FeS_2$ bonds with limonite and $Fe_2(SO4)_4$ being generated. To evaluate the conversion efficiency of each product after 672 h of treatment in the digestion environment, the mineral intensity factor (MIF) method was employed. Each mineral exhibits significant XRD reflection determined under specific experimental conditions. The MIF value is calculated by $\mathrm{MIF} = \left(\frac{I_X}{I_S}\right)\left(\frac{\%S}{\%X}\right)$,[39] where $\%X$ is the mass % of clay mineral X, $\%S$ is the mass % of the standard, $I_X$ is the intensity of clay


https://doi.org/10.1021/acsomega.3c04540
ACS Omega 2023, 8, 35054–35065

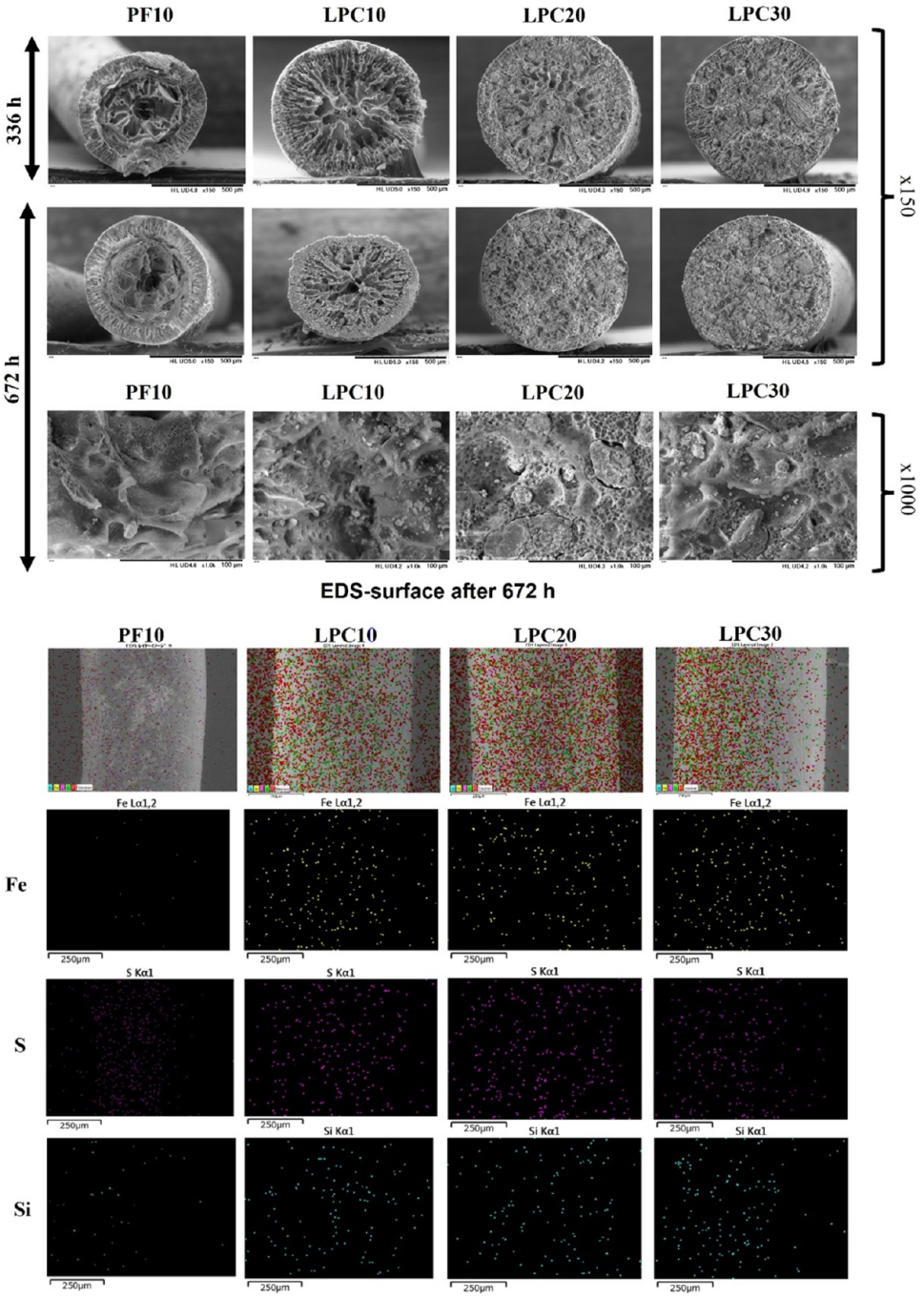


**Figure 6.** SEM images of the cross section of PES and the composite fibers at 150× and 1000× magnifications, and the EDS mapping of Fe, S, and Si elements after 672 h of the digestion process.

mineral X in the XRD pattern of the mixture, and $I_S$ is the intensity of the standard in the XRD pattern of the mixture. The conversion of $FeS_2$ and $Fe_2(SO_4)_3$ was calculated by $\%X = \left(\frac{I_X}{I_S}\right)\left(\frac{M_S}{\mathrm{MIF}}\right)\left(\frac{100}{M}\right)$, where $M_S$ represents the amount of the standard and M is the total mass of the fibers and the added standard. 25 wt % ZnO was used as an internal standard when 75 wt % LPC10 fibers were added to the total mixture amount of 0.4 g. The MIF and conversion values of $Fe_2(SO_4)_3$ and $FeS_2$ are shown in Table 5.

The higher conversion value of $Fe_2(SO_4)_3$ than that of $FeS_2$ indicates that in the presence of water in the anaerobic environment, almost all $H_2S$ is converted to $Fe_2(SO_4)_3$ with 32.4% conversion efficiency, while the conversion efficiency of $FeS_2$ is only 6.8%.

The goethite-rich composite adsorbent demonstrated an enhanced adsorption capacity for $H_2S$ under anaerobic conditions. Therefore, its effectiveness in adsorbing $H_2S$ was evident in the in vitro environment, where $H_2S$ generation was observed.

As mentioned above, CO suppression was also observed in the samples that contained limonite powder and composite fibers. This phenomenon could be attributed to several reactions occurring in the anaerobic environment in the presence of CO, $H_2O$, and limonite during the anaerobic digestion process.


https://doi.org/10.1021/acsomega.3c04540
ACS Omega 2023, 8, 35054−35065

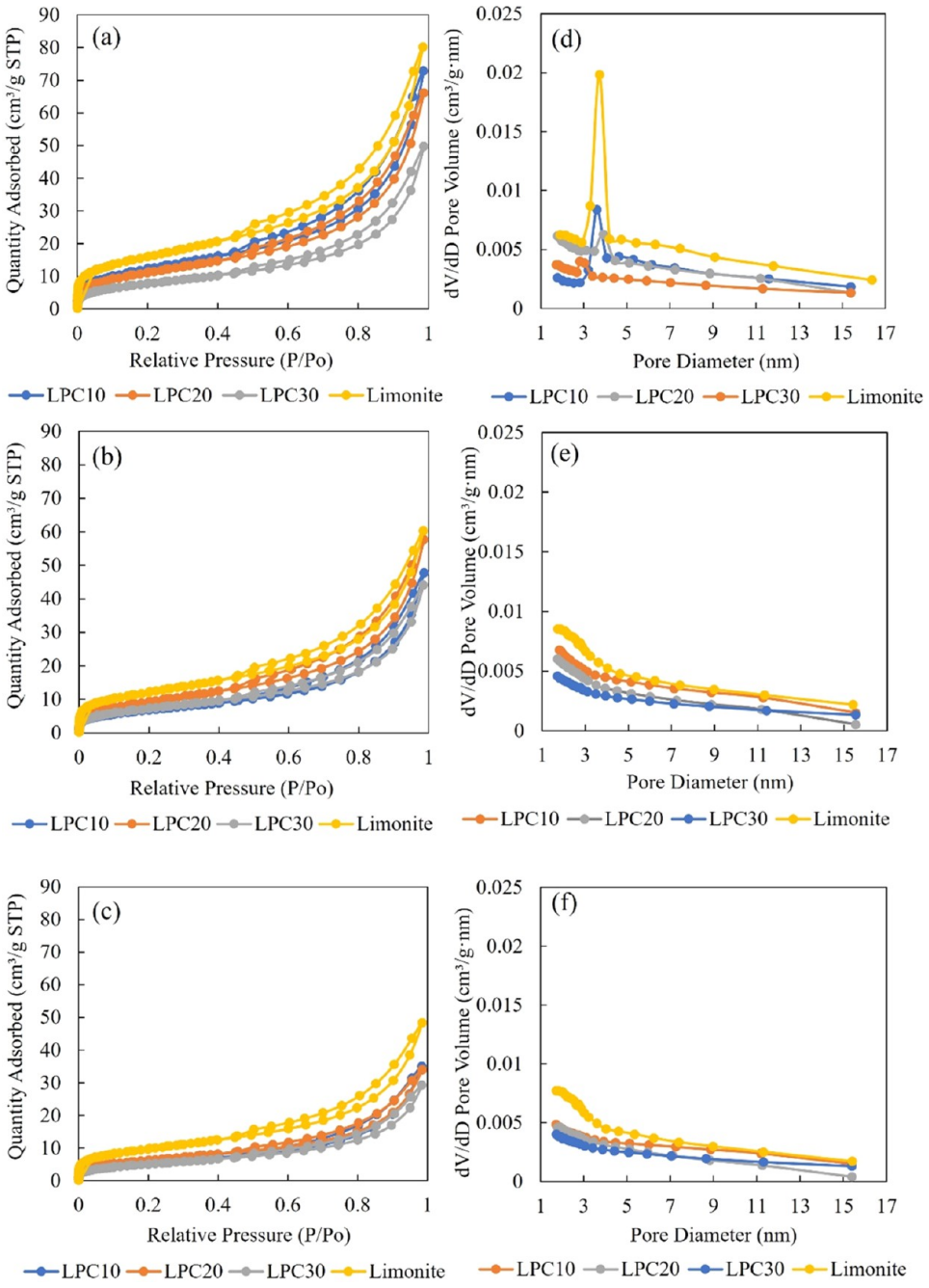


**Figure 7.** $N_2$ adsorption of limonite, PF10, and composite fibers at 0 h (a), 336 h (b), and 672 h (c); and pore size distribution of limonite, PF10, and composite fibers at 0 h (d), 336 h (e), and 672 h (f) of the digestion process.

**Table 4. BET Surface Area, Pore Volume, Pore Size of Limonite, and Elemental Composition of LPC Fibers at 336 and 672 h of the Digestion Process**

| | BET surface area ($m^2/g$) | | BJH adsorption average pore volume ($cm^3/g$) | | BJH adsorption average pore size (nm) | | elemental composition | | | | | |
|---|---|---|---|---|---|---|---|---|---|---|---|---|
| | | | | | | | C/Fe | | Si/Fe | | S/Fe | |
| sample | 336 h | 672 h | 336 h | 672 h | 336 h | 672 h | 336 h | 672 h | 336 h | 672 h | 336 h | 672 h |
| limonite | 39.13 | 13.45 | 0.069 | 0.059 | 4.77 | 5.89 | 0.16 | 0.2 | 0.13 | 0.17 | 0.02 | 0.03 |
| LPC10 | 29.97 | 9.40 | 0.030 | 0.03 | 4.84 | 4.63 | 0.99 | 0.94 | 0.13 | 0.11 | 0.33 | 0.21 |
| LPC20 | 21.10 | 8.70 | 0.038 | 0.041 | 5.08 | 4.90 | 0.94 | 0.94 | 0.11 | 0.13 | 0.33 | 0.21 |
| LPC30 | 23.67 | 8.80 | 0.034 | 0.037 | 5.73 | 5.60 | 1.08 | 0.9 | 0.13 | 0.1 | 0.42 | 0.2 |
| PF10 | 5.56 | 4.80 | 0.010 | 0.006 | 5.19 | 5.19 | | | | | | |

$$FeOOH + H_2S \rightarrow FeS + H_2O \quad (1)$$

$$2CO \rightarrow C + CO_2 \quad (2)$$



https://doi.org/10.1021/acsomega.3c04540
ACS Omega 2023, 8, 35054−35065

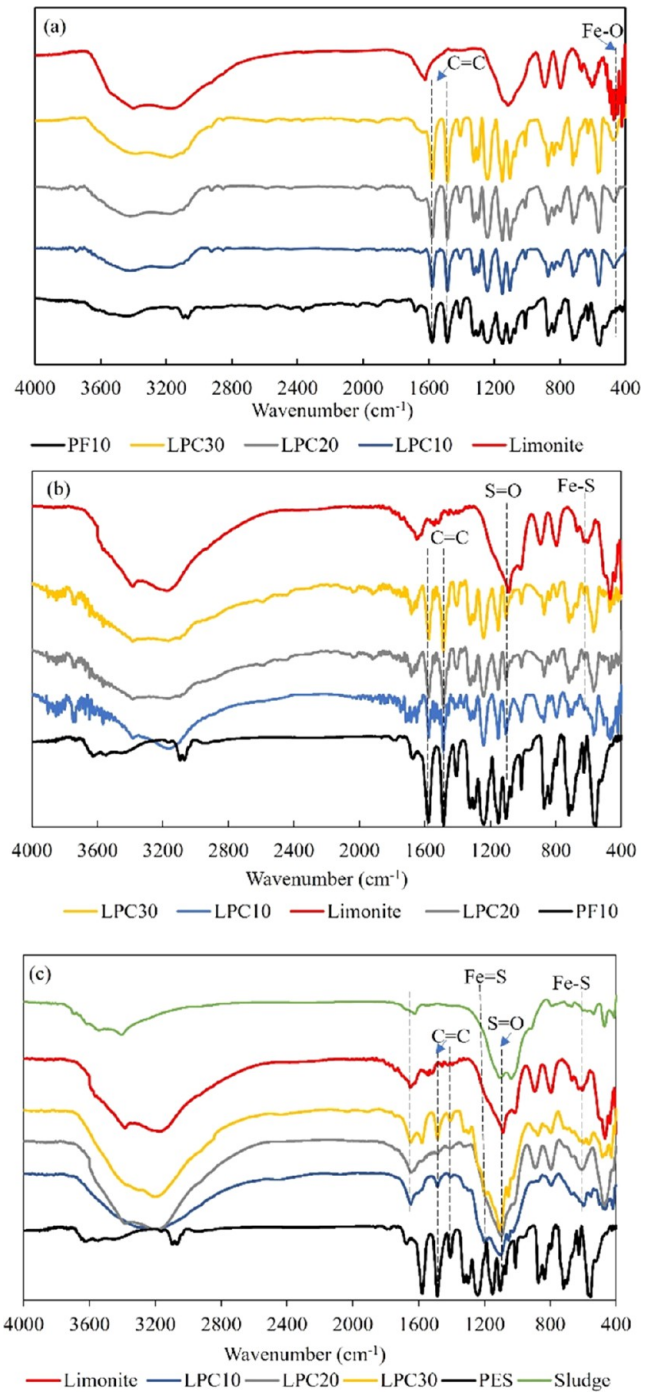


**Figure 8.** FT-IR spectra of limonite, PF10, and the composite fibers at 0 h (a), 336 h (b), and 672 h (c) of the digestion process.

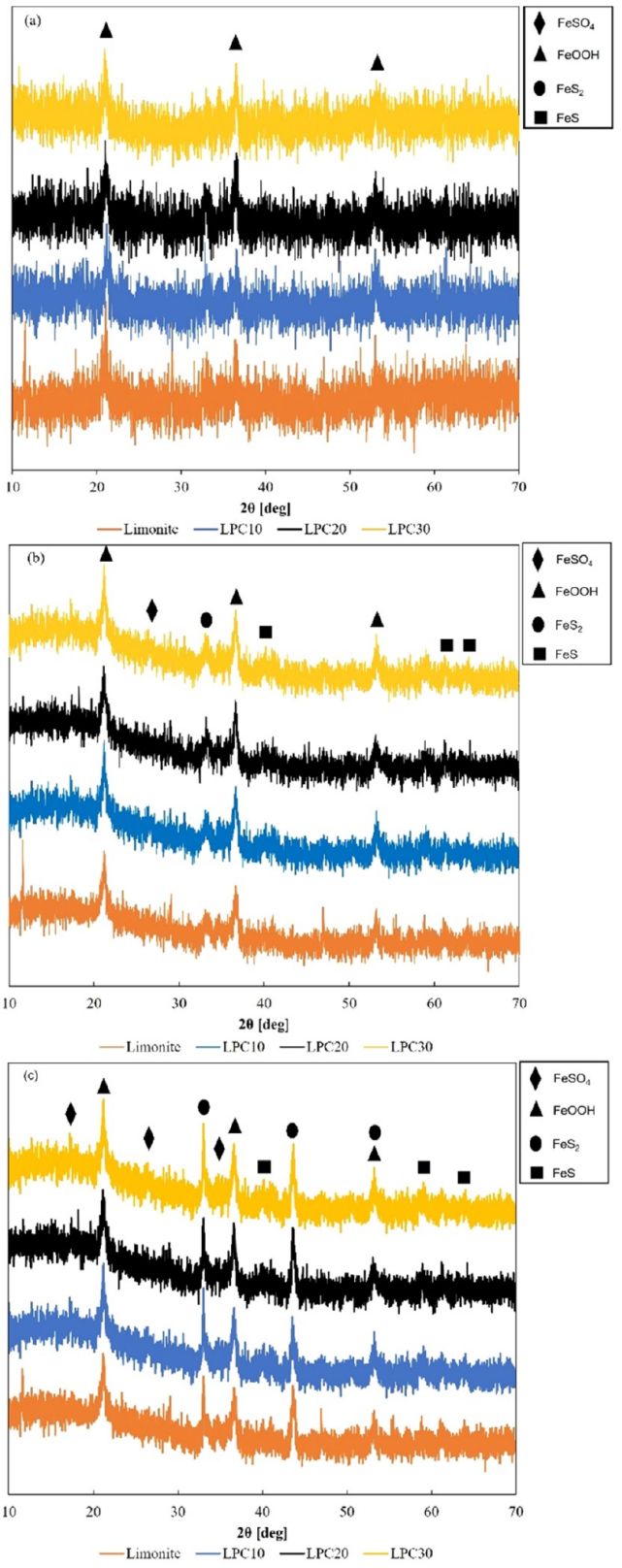


**Figure 9.** XRD pattern of limonite and composite fibers at 0 h (a), 336 h (b), and 672 h (c) of the digestion process.

$$3Fe + 2CO \rightarrow Fe_3C + CO_2 \quad (3)$$

$$CO + H_2O \rightarrow CO_2 + H_2 \quad (4)$$

$$CO + H_2 \rightarrow C + H_2O \quad (5)$$

$$3Fe + C \rightarrow Fe_3C \quad (6)$$

$$Fe_3C + 3H_2S \rightarrow 3FeS + C + 3H_2 \quad (7)$$

$$FeO + H_2S \rightarrow FeS + H_2O \quad (8)$$

$$2FeOOH + 3H_2S + 8H_2O \rightarrow Fe_2(SO_4)_3 + 12H_2 \quad (9)$$

$$FeS + H_2S \rightarrow FeS_2 + H_2 \quad (10)$$

Reaction 1 takes precedence due to its significance in oxidizing $H_2S$, a common byproduct of anaerobic processes. In this reaction, FeOOH acts as an electron acceptor, resulting in the



https://doi.org/10.1021/acsomega.3c04540
ACS Omega 2023, 8, 35054−35065

Table 5. MIF Values Used in This Study and Conversion Efficiency for Significant Reflections

| mineral | reflection position ($2\theta$ deg) | MIF*$_{100}$ | conversion efficiency (%) |
|---|---|---|---|
| $Fe_2(SO_4)_3$ | 21.2[40] | 0.132 | 32.4 |
| $FeS_2$ | 33.2[39] | 0.94 | 6.8 |

formation of iron sulfide (FeS) and water ($H_2O$). This priority of reaction explains the more efficient removal of $H_2S$ gas than that of CO gas in anaerobic environments. Our research further indicates that FeOOH can catalyze the oxidation of CO, providing a pathway for FeOOH to react with CO, as also reported by other researchers.[41,42] Consequently, this interaction can potentially lead to the mitigation of CO gas in sludge environments. This finding highlights the dual role of FeOOH in addressing multiple gas species. On another note, the products in these reactions, FeS, FeO, and $Fe_3C$, generated in reactions 1−3 can undergo reactions 6−8. These reactions involve the reactivity of FeO and $Fe_3C$ with $H_2S$, resulting in the production of FeS. Subsequently, FeS continues to react with $H_2S$ to form $FeS_2$[43,44] as the final product, which is also confirmed by FT-IR and XRD measurements.

## 4. CONCLUSIONS

The wet spinning of limonite-dispersed PES−NMP solution was successfully converted to composite fibers containing goethite, capturing $H_2S$ efficiently. The adsorption mechanism was Langmuir type, and the maximum suppression adsorption amount was 3.7−4.4 g $H_2S$/g, suggesting that the adsorption was due to mesopore adsorption. Using composite fibers and limonite in anaerobic microorganism sludge in vitro digestion showed promising results in reducing $H_2S$ production. CO production generated in anaerobic fermentation was also inhibited, suggesting that coexistence with limonite fibers can also reduce CO in the anaerobic environment. In anaerobic digestion processes, the recovery of limonite fibers led to the analysis of adsorbed $H_2S$, which was then converted to $FeS_2$ and $Fe_2(SO4)_3$ with conversion efficiencies of 6.8 and 32.4%, respectively. Utilization of composite fibers was able to suppress $H_2S$ formation to a low concentration in the anaerobic digestion process at 672−840 h (28−35 days) but increased to 30 ppm at 1176 h (49 days). The degradation of this property was not caused by material degradation of PES but by the loss of the limonite portion that was degraded by reaction with $H_2S$, forming pyrite ($FeS_2$) and ferric sulfate ($Fe_2(SO_4)_3$) as primary products. However, the fibrous form of the material has the advantage that it can be removed and replaced, indicating that the material is close to practical use.

## AUTHOR INFORMATION


### Corresponding Author

**Takaomi Kobayashi** − *Department of Science and Technology Innovation, Nagaoka University of Technology, Nagaoka 940-2188, Japan;* orcid.org/0000-0001-7649-4607; Email: takaomi@vos.nagaokaut.ac.jp

### Authors

**Anh Phuong Le Thi** − *Department of Science and Technology Innovation, Nagaoka University of Technology, Nagaoka 940-2188, Japan*

**Reiko Wakasugi** − *Department of Biochemical System Engineering, National Institute of Technology, Kumamoto College, Yatsushiro, Kumamoto 866-8501, Japan*

Complete contact information is available at: https://pubs.acs.org/10.1021/acsomega.3c04540


### Notes

The authors declare no competing financial interest.

## ACKNOWLEDGMENTS

The authors would like to extend their heartfelt appreciation to all the members of the Kobayashi Laboratory and the Analysis Center at Nagaoka University of Technology for their invaluable assistance in conducting the XRD measurements and other experiments throughout the entire research process. Their support has been instrumental in the successful completion of this study. Furthermore, the authors confirm that this research did not receive any specific grants from funding agencies in the public, commercial, or not-for-profit sectors.

## REFERENCES


(1) Chou, C. H. S. J.; World Health Organization. *Hydrogen Sulfide: Human Health Aspects*; World Health Organization: Geneva, 2003.

(2) Hadi, A.; Mat, R.; Somderam, S.; Abd Aziz, A. S.; Mohamed, A. Hydrogen Sulfide Adsorption by Zinc Oxide-Impregnated Zeolite (Synthesized from Malaysian Kaolin) for Biogas Desulfurization. *J. Ind. Eng. Chem.* **2018**, *65*, 334−342.

(3) Dunnette, D. A.; Chynoweth, D. P.; Mancy, K. H. The Source of Hydrogen Sulfide in Anoxic Sediment. *Water Res.* **1985**, *19*, 875−884.

(4) Watanabe, M.; Higashioka, Y.; Kojima, H.; Fukui, M. Proposal of Desulfosarcina Ovata Subsp. Sediminis Subsp. Nov., a Novel Toluene-Degrading Sulfate-Reducing Bacterium Isolated from Tidal Flat Sediment of Tokyo Bay. *Syst. Appl. Microbiol.* **2020**, *43*, No. 126109.

(5) Sakai, S.; Nakaya, M.; Takayasu, K. Hydrogen Sulfide Distribution in Bottom and Pore Waters during an Anoxic Period in Lake Nakaumi, Japan. *Laguna* **2004**, *11*, 65−68.

(6) Morii, D.; Miyagatani, Y.; Nakamae, N.; Murao, M.; Taniyama, K. Japanese Experience of Hydrogen Sulfide: The Suicide Craze in 2008. *J. Occup. Med. Toxicol.* **2010**, *5*, No. 28.

(7) Nogué, S.; Pou, R.; Fernández, J.; Sanz-Gallén, P. Fatal Hydrogen Sulphide Poisoning in Unconfined Spaces. *Occup. Med.* **2011**, *61*, 212−214.

(8) Mooyaart, E. A. Q.; Gelderman, E. L. G.; Nijsten, M. W.; de Vos, R.; Hirner, J. M.; de Lange, D. W.; Leuvenink, H. D. G.; van den Bergh, W. M. Outcome after Hydrogen Sulphide Intoxication. *Resuscitation* **2016**, *103*, 1−6.

(9) Tanada, S.; Boki, K. Properties of Various Adsorbents for Removal of Hydrogen Sulfide Gas. *Chem. Pharm. Bull.* **1974**, *22*, 2703−2709.

(10) Shah, M. S.; Tsapatsis, M.; Siepmann, J. I. Hydrogen Sulfide Capture: From Absorption in Polar Liquids to Oxide, Zeolite, and Metal−Organic Framework Adsorbents and Membranes. *Chem. Rev.* **2017**, *117*, 9755−9803.

(11) Balsamo, M.; Cimino, S.; de Falco, G.; Erto, A.; Lisi, L. ZnO-CuO Supported on Activated Carbon for H2S Removal at Room Temperature. *Chem. Eng. J.* **2016**, *304*, 399−407.

(12) Magnone, E.; Kim, S. D.; Park, J. H. A Systematic Study of the Iron Hydroxide-Based Adsorbent for Removal of Hydrogen Sulphide from Biogas. *Microporous Mesoporous Mater.* **2018**, *270*, 155−160.

(13) Raabe, T.; Mehne, M.; Rasser, H.; Krause, H.; Kureti, S. Study on Iron-Based Adsorbents for Alternating Removal of H2S and O2 from Natural Gas and Biogas. *Chem. Eng. J.* **2019**, *371*, 738−749.

(14) Ko, T.-H.; Chu, H.; Lin, H.-P.; Peng, C.-Y. Red Soil as a Regenerable Sorbent for High Temperature Removal of Hydrogen Sulfide from Coal Gas. *J. Hazard. Mater.* **2006**, *136*, 776−783.




https://doi.org/10.1021/acsomega.3c04540
*ACS Omega* 2023, 8, 35054−35065

(15) Cao, Y.; Hu, X.; Lin, X.; Lin, Y.; Huang, R.; Jiang, L.; Wei, K. Low-Temperature Desulfurization on Iron Oxide Hydroxides: Influence of Precipitation Ph on Structure and Performance. *Ind. Eng. Chem. Res.* **2015**, *54*, 2419−2424.
(16) Lee, S.; Lee, T.; Kim, D. Adsorption of Hydrogen Sulfide from Gas Streams Using the Amorphous Composite of α-FeOOH and Activated Carbon Powder. *Ind. Eng. Chem. Res.* **2017**, *56*, 3116−3122.
(17) Mrosso, R.; Machunda, R.; Pogrebnaya, T. Removal of Hydrogen Sulfide from Biogas Using a Red Rock. *J. Energy* **2020**, *2020*, No. 2309378.
(18) Zhou, Q.; Jiang, X.; Li, X.; Jiang, W. The Control of H2S in Biogas Using Iron Ores as in Situ Desulfurizers during Anaerobic Digestion Process. *Appl. Microbiol. Biotechnol.* **2016**, *100*, 8179−8189.
(19) Toda, K.; Tanaka, T.; Tsuda, Y.; Ban, M.; Koveke, E. P.; Koinuma, M.; Ohira, S.-I. Sulfurized Limonite as Material for Fast Decomposition of Organic Compounds by Heterogeneous Fenton Reaction. *J. Hazard. Mater.* **2014**, *278*, 426−432.
(20) Iguchi, Y.; Itoh, Y. Sulfur Sorption Rate and Equilibrium Content of Reduced Iron in H2-H2S Mixtures. *Isij Int.* **2004**, *44*, 250−256.
(21) TANAKA, T.; KOGA, T.; CHIKUSHI, H.; OHIRA, S.-I.; HASEGAWA, A.; TODA, K. Dynamic Evaluation on Hydrogen Sulfide Adsorption Properties of Solid Adsorbents Using Their 'Sink Efficiencies' − in Case of Desulfurization by Limonite. *Bunseki Kagaku* **2011**, *60*, 641−646.
(22) Lee, S.; Lee, T.; Kim, D. Adsorption of Hydrogen Sulfide from Gas Streams Using Amorphous Composite of α-FeOOH and Activated Carbon Powder. *Ind. Eng. Chem. Res.* **2017**, *56*, 3116−3122.
(23) Kobayashi, T.; Ohshiro, M.; Nakamoto, K.; Uchida, S. Decontamination of Extra-Diluted Radioactive Cesium in Fukushima Water Using Zeolite-Polymer Composite Fibers. *Ind. Eng. Chem. Res.* **2016**, *55*, 6996−7002.
(24) Wang, X.; Ma, X.; Sun, L.; Song, C. A Nanoporous Polymeric Sorbent for Deep Removal of H2S from Gas Mixtures for Hydrogen Purification. *Green Chem.* **2007**, *9*, 695−702.
(25) Nakamoto, K.; Ohshiro, M.; Kobayashi, T. Mordenite Zeolite - Polyethersulfone Composite Fibers Developed for Decontamination of Heavy Metal Ions. *J. Environ. Chem. Eng.* **2017**, *5*, 513−525.
(26) Nakamoto, K.; Ohshiro, M.; Kobayashi, T. Continuous Flow Column Adsorption of Mordenite Zeolite−Polymer Compositfibers for Lead Removal. *Desalin. Water Treat.* **2018**, *109*, 297−306.
(27) Ooshiro, M.; Kobayashi, T.; Uchida, S. Fibrous Zeolite-Polymer Composites for Decontamination of Radioactive Waste Water Extracted from Radio-Cs Fly Ash. *Int. J. Eng. Tech. Res.* **2017**, *7*, No. 265044.
(28) Nakamoto, K.; Kobayashi, T. Fibrous Mordenite Zeolite - Polymer Composite Adsorbents to Methylene Blue Dye **2017** *7* 264902.
(29) Nakajima, L.; Yusof, N. N. M.; Kobayashi, T. Calixarene-Composited Host−Guest Membranes Applied for Heavy Metal Ion Adsorbents. *Arab. J. Sci. Eng.* **2015**, *40*, 2881−2888.
(30) Fauteux-Lefebvre, C.; Abatzoglou, N.; Blais, S.; Braidy, N.; Hu, Y. Iron Oxide-Functionalized Carbon Nanofilaments for Hydrogen Sulfide Adsorption: The Multiple Roles of Carbon. *Carbon* **2015**, *95*, 794−801.
(31) Bagreev, A.; Rahman, H.; Bandosz, T. J. Study of H2S Adsorption and Water Regeneration of Spent Coconut-Based Activated Carbon. *Environ. Sci. Technol.* **2000**, *34*, 4587−4592.
(32) Yu, Z.; Wang, X.; Hou, Y. N.; Pan, X.; Zhao, Z.; Qiu, J. Nitrogen-Doped Mesoporous Carbon Nanosheets Derived from Metal-Organic Frameworks in a Molten Salt Medium for Efficient Desulfurization. *Carbon* **2017**, *117*, 376−382.
(33) Pan, Y.; Chen, M.; Hu, M.; Tian, M.; Zhang, Y.; Long, D. Probing the Room-Temperature Oxidative Desulfurization Activity of Three-Dimensional Alkaline Graphene Aerogel. *Appl. Catal., B* **2020**, *262*, No. 118266.
(34) Khabbaz, M.; Entezari, M. H. Simple and Versatile One-Step Synthesis of FeS2 Nanoparticles by Ultrasonic Irradiation. *J. Colloid Interface Sci.* **2016**, *470*, 204−210.
(35) Vernekar, D.; Jagadeesan, D. Tunable Acid-Base Bifunctional Catalytic Activity of FeOOH in an Orthogonal Tandem Reaction. *Catal. Sci. Technol.* **2015**, *5*, 4029−4038.
(36) Stojilovic, N.; Isaacs, D. E. Inquiry-Based Experiment with Powder XRD and FeS2Crystal: "Discovering" the (400) Peak. *J. Chem. Educ.* **2019**, *96*, 1449−1452.
(37) Ma, S.; Cai, Q.; Lu, K.; Liao, F.; Shao, M. Bi-Functional Au/FeS (Au/Co3O4) Composite for in Situ SERS Monitoring and Degradation of Organic Pollutants. *J. Nanopart. Res.* **2016**, *18*, No. 26.
(38) Persson, K. *Materials Data on BaSO4 (SG: 62) by Materials Project*, Lawrence Berkeley National Lab.
(39) Środoń, J.; Drits, V. A.; McCarty, D. K.; Hsieh, J. C. C.; Eberl, D. D. Quantitative X-Ray Diffraction Analysis of Clay-Bearing Rocks from Random Preparations. *Clays Clay Miner.* **2001**, *49*, 514−528.
(40) Yao, J.; Jin, T.; Li, Y.; Xiao, S.; Huang, B.; Jiang, J. Electrochemical Performance of Fe2(SO4)3 as a Novel Anode Material for Lithium-Ion Batteries. *J. Alloys Compd.* **2021**, *886*, No. 161238.
(41) Tsubouchi, N.; Mochizuki, Y.; Byambajav, E.; Takahashi, S.; Hanaoka, Y.; Ohtsuka, Y. Catalytic Performance of Limonite Ores in the Decomposition of Model Compounds of Biomass-Derived Tar. *Energy Fuels* **2017**, *31*, 3898−3904.
(42) Mochizuki, Y.; Ogawa, A.; Tsubouchi, N. Removal of Hydrogen Sulfide and Ammonia by Goethite-Rich Limonite in the Coexistence of Coke Oven Gas Components. *ISIJ Int.* **2017**, *57*, 435−442.
(43) Kim, H. T.; Nguyen, T. P. N.; Kim, C. D.; Park, C. Formation Mechanisms of Pyrite (FeS2) Nano-Crystals Synthesized by Colloidal Route in Sulfur Abundant Environment. *Mater. Chem. Phys.* **2014**, *148*, 1095−1098.
(44) Thiel, J.; Byrne, J. M.; Kappler, A.; Schink, B.; Pester, M. Pyrite Formation from FeS and H 2 S Is Mediated through Microbial Redox Activity. *Proc. Natl. Acad. Sci. U.S.A.* **2019**, *116*, 6897−6902.


https://doi.org/10.1021/acsomega.3c04540
*ACS Omega* 2023, 8, 35054−35065